Experiments and Simulations of Infrared Transmission by Transverse Magnetic Mode through Au Gratings on Silicon with Various Air-slot Widths over the Period

Yan-Ru Chen*, and C. H. Kuan

Graduate Institute of Electronics Engineering and Department of electric engineering, National Taiwan University, Taipei, Taiwan, Republic of China

*e-meal:d93943029@ntu.edu.tw

ABSTRACT

Au gratings with various air-slot widths were fabricated by electron beam lithography system (e-beam) and their infrared (2.5~25μm) transmission of the transverse magnetic mode (TM mode) were investigated by the Fourier Transform Infrared Spectroscopy (FTIR). Simulations were used theoretically by the Maxwell equations and the surface impedance boundary condition (SIBC) method. Simulation results explain the relationship between surface plasma and transmission dips.

Keywords: gratings, e-beam, infrared

1 INTRODUCTION

Transmission through one-dimensional metallic gratings has been researched for decades because of their optical characteristics and potential applications in various fields, including beam splitting polarizers and photo-detectors. Advanced nano-technologies that can realize sub-wavelength metal/dielectric structures and the development of calculation methods to analyze their electromagnetic properties have all contributed to the understanding and application of metallic gratings. It is the purpose of this paper to demonstrate experimentally and simulate theoretically the infrared transmission by the transverse magnetic mode (TM mode) through Au gratings with various air-slot widths. Au gratings with various air-slot widths are fabricated on silicon substrate by electron beam lithography system (e-beam), and infrared transmittance (2.5~25μm) by transverse electric mode (TM-mode) are investigated by Fourier Transform Infrared Spectroscopy (FTIR). Moreover, the Maxwell equations and surface impedance boundary condition (SIBC) were used to simulate the transmission through Au gratings with various air-slot widths. Simulation results agree with experiments and support the *surface plasma theory*.

2 EXPERIMENT

At first, the e-beam, which was provided by ELIONIX, was used to pattern various air-slot widths of Au gratings on silicon substrate. In order to measure the whole transmission through gratings, the total area of the Au gratings had to be larger than 2mm×2mm to meet the minimum FTIR spot size. 10nA beam current was used in order to dramatically shorten the exposing time. In our experiment, the area of 3.6mm×3.6mm was exposed after the spin-coated of ZEP520A (e-beam resist). 20nm Au film was evaporated on the sample after develop. Then ZDMAC was used to lift off the un-patterned parts. The fabrication procedures are shown in the sub-plot of Figure 1. In our following experiments, the period of Au gratings was always 4μm. The thickness of Au was always 20nm, which is larger than the skin depth of Au (~10 nm) to prevent the infrared from transmitting. The scanning electron microscopy (SEM), which is provided by ELIONIX, used to observe the plain view of Au gratings. Figure 1 shows the SEM picture of Au gratings with 34% air-slot width on silicon substrate. After the fabrication process, the FTIR system (IFS 66v/S), which was provided by Bruker, was finally used to investigate the TM-mode infrared transmittance of the sample, as shown in the schematic set-up of Figure 2. In this system, infrared is normal incident to the Au gratings. It is noticed that bare silicon substrate is as our reference, so the measured grating transmission was divided by that of bare silicon. In Figure 3 shows the experimental infrared transmission of Au gratings with various air-slot widths, which is already divided by that of bare silicon. The x-axis represents the wavelength (2.5μm~25μm), and the y-axis represents transmission. The percentage of the air-slot width over the period of 4μm, from 25% to 91% (along the dashed lines), is shown by various solid-lines.

3 SIMULATIONS

The Maxwell equations and the surface impedance boundary condition (SIBC) method[3] are both used to simulate the TM-mode infrared transmittance through Au-gratings with various air-slot widths. Figure 2 demonstrates the coordinates and parameters in simulation below. Boundary conditions,

$$E_{\parallel} = i(Z/k_0)\vec{n} \times H_{\parallel}$$

, are applied to relating tangential components of electric and magnetic fields at Au/dielectric interface, where Z is $1/n_{metal}$ with n_{metal} being the refraction index of the metal[4], k_0 is the wavenumber of the incident light, which is equal to $2\pi/\lambda$ with λ being wavelength of incident light, and $\vec{n}$ is a dimensionless unit vector, which direction is outward to the Au surface. Because the total area of Au gratings is lager than the FTIR spot size, wave functions outside the gratings can be considered as the plain wave. Figure 2 illustrates the definition of coordinates and the related parameters in later simulation. The tangential

electric fields in various regions are expressed as a linear combination of orthogonal modes as follows:

tangential magnetic fields in region 1:

$$\exp(-ik_{y,0,1}(y-h/2))+\sum_{n=-\infty}^{\infty}R_n\exp\{i[k_{x,n,1}x+k_{y,n,1}$$

tangential magnetic fields in region 2:

$$\sum_{m=1}^{\infty}X_m(x)Y_m(y)=\sum_{m=1}^{\infty}[d_m\sin(k_{x,m,2}x)+\cos(k_{x,m,2}x)][a_m$$

with

$$X_m(x)=d_m\sin(k_{x,m,2}x)+\cos(k_{x,m,2}x)$$

and

$$Y_m(y)=a_m\exp[i(k_{y,m,2})y]+b_m\exp[-i(k_{y,m,2})y]$$

tangential magnetic fields in region 3:

$$\sum_{n=-\infty}^{\infty}T_n\exp\{i[k_{x,n,3}x-k_{y,n,3}(y+h/2)]\}$$

where

p is the period of gratings,

h is the Au thickness,

ε_i is the dielectric constant of region *i*,

$k_{x,n,i}$ is the *n*th mode x-direction wavenumber in region *i* (*i* =1,2, or 3),

$k_{y,n,i}=\sqrt{\varepsilon_i k_0^2-k_{x,n,i}^2}$ is *n*th mode y-direction wavenumber in region *i* (*i* =1, 2, or 3),

a_m/b_m is the magnitude of +y/-y direction wave at *y*=0 in region 2 (*m*=1, 2, 3…), and

R_n/T_n is the *n*th mode reflectance/transmission coefficient (*n*=0, ± 1, ± 2, ± 3…).

Because the period of Au gratings is *p*, $k_{x,n,1}$ and $k_{x,n,3}$ are equal to $2n\pi/p$ in region 1 and 3. d_m is *m*th mode coefficient which will be determined below. ε_1 and ε_2 are the dielectric constant of air, which are equal to 1. ε_3 is the dielectric constant of silicon, which is equal to 11.7.

Applying SIBC to the left-hand and right-hand side of Au/air interface results:

$$d_m=(k_0\varepsilon_2 Z/i)/k_{x,m,2}$$ -------- Eq. 1

and

$$\tan(dk_{x,m,2})=2k_{x,m,2}(k_0\varepsilon_2 Z/i)/[k_{x,m,2}^2-(k_0\varepsilon_2 Z/i)^2]$$

-------- Eq. 2

It is known that $k_{x,m,2}$ $(m=2,3...)$ has a solution near $(m-1)\pi/d$ but not $(m-1)\pi/d$, so $k_{x,m,2}$ $(m=2,3...)$ can be found easily by Newton method. An important step is to find $k_{x,1,2}$. $k_{x,1,2}$ is near zero but not zero. We use Taylor series expanded at $k_{x,1,2}$=0 in Eq. 2 and get

$$dk_{x,1,2}=2k_{x,1,2}(k_0\varepsilon_2 Z/i)/[k_{x,1,2}^2-(k_0\varepsilon_2 Z/i)^2]$$

, in which an approximate $k_{x,1,2}$ can be easily found. The found $k_{x,1,2}$ above is used as initial value of the Newton method and we can get more precise $k_{x,1,2}$. Thus we can get $k_{x,m,2}$ (m=1, 2, 3...). Equating the tangential electric and magnetic fields and applying the SIBC conditions at y=*h*/2 and *y* =-*h* / 2 yields the following four equations:

$$1+\sum_{n=-\infty}^{\infty}R_n\exp[i(2n\pi x/p)]=\sum_{m=1}^{\infty}X_m(x)(\varphi_m a_m+\varphi_m^{-1}b_m),\ 0\le x\le d$$

-------- Eq. 3

$$-ik_{y,0,1}+\sum_{n=-\infty}^{\infty}ik_{y,n,1}R_n\exp[i(2n\pi x/p)]=\begin{cases}\sum_{m=1}^{\infty}X_m(x)k_{y,m,2}(\varphi_m a_m-\varphi_m^{-1}b_m),\ 0\le x\le d\\(k_0\varepsilon_1 Z/i)\{1+\sum_{n=-\infty}^{\infty}R_n\exp[i(2n\pi x/p)]\},\ d\le x\le p\end{cases}$$

-- Eq. 4

$$\sum_{n=-\infty}^{\infty}T_n\exp[i(2n\pi x/p)]=\sum_{m=1}^{\infty}X_m(x)(\varphi_m^{-1}a_m+\varphi_m b_m),\ 0\le x\le d$$

-------- Eq. 5

$$\sum_{n=-\infty}^{\infty} -ik_{y,n,3}T_n \exp[i(2n\pi x/p)] = \begin{cases} \sum_{m=1}^{\infty} iX_m(x)k_{y,m,2}(\varphi_m^{-1}a_m - \varphi_m b_m), & 0 \le x \le d \\ (k_0\varepsilon_1 Z/i)\sum_{n=-\infty}^{\infty} T_n \exp[i(2n\pi x/p)], & d \le x \le p \end{cases}$$

-------- Eq. 6

where $\varphi_m = \exp(ik_{y,m,2}h/2)$.

Thus R_n, T_n, a_m, and b_m can be determined from above equations. Taking the power into consideration, the total power is $|T_0|^2 \times \sqrt{\varepsilon_3}$. Finally the total power is divided by the theoretical transmission of air/silicon interface, $(4\sqrt{\varepsilon_1}\sqrt{\varepsilon_3})/(\sqrt{\varepsilon_1}+\sqrt{\varepsilon_3})^2$, and final results are shown in Figure 4. From Figure 3 and 4, it is observed that experimental and simulation results are matched. The results obtained above are checked using another method that assumes that the Au/dielectric interface is perfectly conducting. It is found that $|T_0|$ will approach to zero as the mode number is very large. So the SIBC method is more suitable and convergent for calculating infrared transmission through Au gratings with various air-slot widths over the period, compared with the method that assuming Au is a perfect conductor. In the above simulation, the waves in region 1 and 3 are defined as *evanescent waves when* $k_{y,n,i}$ *is an image number* and as *propagation waves when* $k_{y,n,i}$ *is a real number*. Because of their exponential-decayed-in-y-axis properties, they can not be detected by the FTIR photo-detector when their transmission is investigated, as shown in Figure 2. Only the *propagation waves* are considered in Figure 4 because of their propagation properties.

4 DISCUSSION

Simulation results explain the relationship between surface plasma and transmission dips. The major two transmission dips are at the wavelength of 4μm and 13.7μm, respectively at b and e in Figure 3 and 4. At first, the 4μm transmission dip is discussed. In Figure 5, the simulated $|R_0|^2$, $|T_0|^2$, $|R_1|^2$, $|T_1|^2$, $|a_0|^2$, and $|b_0|^2$ versus wavelength of 53% air-slot width over Au gratings in the wavelength 2.5μm to 5.5μm are demonstrated. It is noticed that $|T_0|^2$ and $|T_1|^2$ are divided by the transmission of bare silicon, and $|a_0|^2$ and $|b_0|^2$ are very close and represented by black-solid line. In Figure 5, the a and c (at around 4μm but not 4μm) represents the incident waves transmit through the gratings by the waves with coefficients T_0 and T_1. At a and c, R_1 is approach to zero thus no surface plasma on the air side is induced. At b, $|R_1|^2$ is much lager than a and b, and $|T_0|^2$, $|T_1|^2$, $|a_0|^2$, and $|b_0|^2$ are approach to zero. Surface plasma on the air side is induced at b (4μm). In Figure 6, it shows the schematic of the transition between a, b and c. The arrows represent the waves, and the length of arrows represents the amplitude of the waves. Most incident light can transmit through the gratings at a and c. At b, $|R_1|^2$ is enhanced in a large quantity. The waves with coefficients a_0, b_0, T_0 and T_1 are approach to zero. Surface plasma on the air side is induced at b. The same story happens at transition d, e, and f in Figure 3 and 4. Figure 7 shows the schematic of the transition between d, e, and f. It is shown that the waves with coefficients R_1 are always approach zero. No waves with coefficients R_1 are induced. At e, the waves with coefficients T_1 are induced and the surface plasma on the silicon side is induced. Thus, our results support the surface plasma theory.

5 SUMMARY

To sum up, Au gratings on silicon substrate with various air-slot widths over the period were fabricated experimentally by e-beam and evaporator. The infrared (2.5μm~25μm) transmission through Au gratings was investigated by FTIR system. Furthermore, the Maxwell equations and the surface impedance boundary condition (SIBC) method were used to simulate the experimental results. Simulation results explain the relationship between surface plasma and transmission dips. These experimental and theoretical results can contribute to the understanding of TM-mode infrared transmission properties of metal gratings and the application on the field of infrared photo-detectors, bio-chip sensor, and light-emitting diode polarizers.

REFERENCES

[1] F. J. Garcia-Vidal and L. Martin-Moreno, "Transmission and focusing of light in one-dimensional periodically nanostrucutred metals," Phys. Rev. B 66, 155412(1) -155412(10) (2002)

[2] J. M. Steele, C. E. Moran, A. Lee, C. M. Aguirre, and N. J. Halas, "Metallodielectric gratings with subwavelength slots: Optical properties," PHYSICAL REVIEW B 68, 205103 (2003)

[3] David Crouse and Pavan Keshavareddy, "Polarization independent enhanced optical transmission in one-dimensional gratings and device applications," OPTICS EXPRESS, Vol. 15, No. 4, 1415

[4] M. A. Ordal, L. L. Long, R. J. Bell, S. E. Bell, R. R. Bell, R. W. Alexander, Jr., and C. A. Ward, "Optical properties of the metals Al, Co, Cu, Au, Fe, Pb, Ni, Pd, Pt, Ag, Ti, and W in the infrared and far infrared," 1 April 1983 / Vol. 22, No. 7 / APPLIED OPTICS

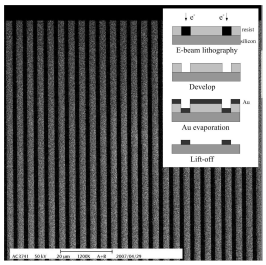

Figure 1: Scanning electron microscopy (SEM) picture of Au gratings with 34% air-slot width on silicon substrate
Sub-plot of Figure 1: Fabrication process of Au gratings on silicon substrate by e-beam and evaporator

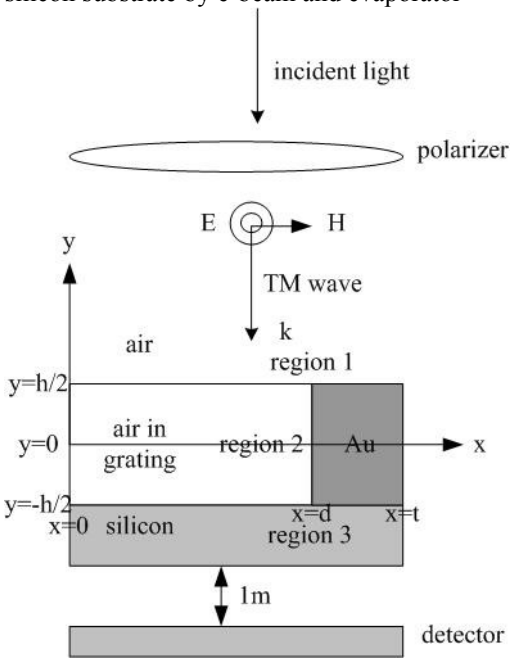

Figure 2: Illustration of infrared transmission measurement and definition of coordinate and parameters in simulation

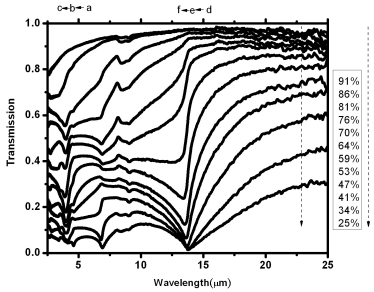

Figure 3: Experimental results of infrared transmission through Au gratings

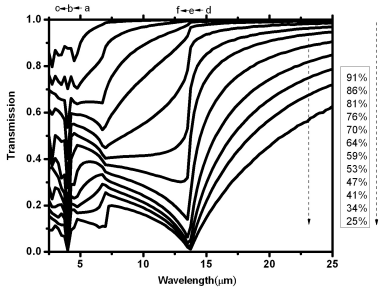

Figure 4: Simulation results of infrared transmission through Au gratings

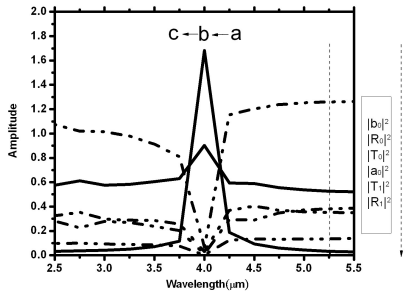

Figure 5: the calculated $|R_0|^2$, $|T_0|^2$, $|R_1|^2$, $|T_1|^2$, $|a_0|^2$, and $|b_0|^2$ versus wavelength of 53% air-slot width

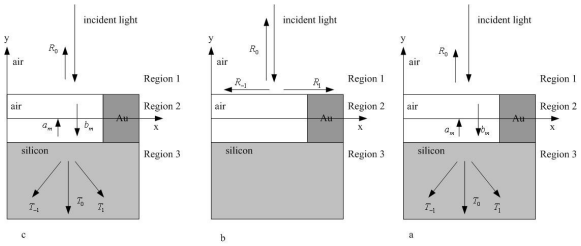

Figure 6: The schematic of the transition between a, b, and c

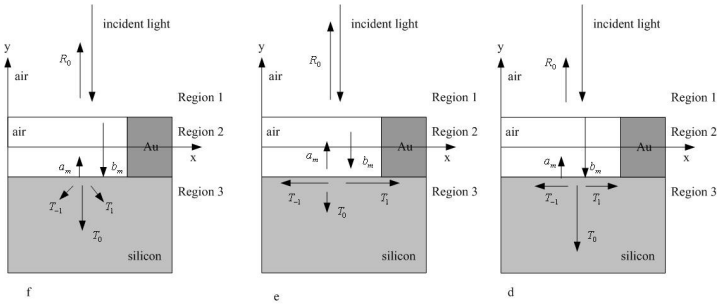

Figure 7: The schematic of the transition between d, e, and f